Final Draft
of the original manuscript:

Zhang, Y.; Feyerabend, F.; Tang, S.; Hu, J.; Lu, X.; Blawert, C.; Lin, T.:
A study of degradation resistance and cytocompatibility of super-hydrophobic coating on magnesium
In: Materials Science and Engineering C (2017) Elsevier

DOI: 10.1016/j.msec.2017.04.057

A study of degradation resistance and cytocompatibility of super-hydrophobic coating on magnesium

Yufen Zhang[a], Frank Feyerabend[b], Shawei Tang[a], Jin Hu [a,*], Xiaopeng Lu[b], Carsten Blawert[b], Tiegui Lin[a].

[a] School of Materials Science and Engineering, Harbin Institute of Technology, Harbin 150001, P.R. China

[b]Institute of Materials Research, Helmholtz-Zentrum Geesthacht Zentrum für Material- und Küstenforschung GmbH, Max-Plank-Str. 1, 21502 Geesthacht, Germany

Abstract

Calcium stearate based super-hydrophobic coating was deposited on plasma electrolytic oxidation (PEO) pre-treated magnesium substrate. The pre-treated magnesium and super-hydrophobic coating covered sample were characterized by scanning electron microscopy, X-ray diffraction and electrochemical corrosion measurements. The cytocompatibility and degradation resistance of magnesium, pre-treated magnesium and super-hydrophobic coating were analysed in terms of cell adhesion and osteoblast differentiation. The results indicate that the calcium stearate top coating shows super-hydrophobicity and that the surface is composed of micro/nanostructure. The super-hydrophobic coating covered sample shows higher barrier properties compared with the PEO pre-treated magnesium and bare magnesium. Human osteoblast proliferation, but not differentiation is enhanced by the PEO coating. Contrary, the super-hydrophobic coating reduces proliferation, but enhances differentiation of osteoblast, observable by the formation of hydroxyapatite. The combination of corrosion protection and cell reaction indicates that this system could be interesting for biomedical applications.

* Corresponding author. BOX 433, School of Materials Science and Engineering, Harbin Institute of Technology, Harbin 150001, P.R. China.
Tel.: +86 451 86415894; Fax: +86 451 86413921.
E-mail address: hujin@hit.edu.cn (J. Hu)

Keywords: Magnesium; super-hydrophobic coating; degradation resistance; cytocompatibility

1. Introduction

Magnesium and its alloys show potential value as a class of biodegradable implant materials [1]. This is because they are biodegradable, exhibit mechanical properties similar to bone, and are physiologically compatible [1, 2], as well as showing osteoinductive behaviour [3, 4]. In the human body, Mg^{2+} is one of the most abundant cations and is essential to all living cells [5]. The density of magnesium (1.74 g/cm^3) is similar to that of natural bone. The elastic modulus of magnesium (42 GPa) is closer to that of bone compared with conventional implant materials, which can avoid stress shielding and osteopenia [6]. The biodegradability of magnesium and its alloys in the body environment avoids the second surgery for temporary implants. Mg and its alloys show more appropriate mechanical properties compared with other degradable materials, such as polymers and ceramics [7]. However, the poor corrosion resistance of commercially pure magnesium and its alloy restricts their wide application as a biomaterial [8].

Recently, the focus of research lies on the control of the degradation of magnesium and magnesium alloys targeted for temporary applications in the biomedical field. In this regard, many magnesium alloys (for example, Mg-Ca, Mg-Zn, Mg-Mn-Zn and Mg-Sr alloys etc.) have been adapted for biomaterial applications [9-11]. These magnesium alloys showed good biocompatibility, but the too high initial degradation rate of magnesium alloys would be a major obstacle for the clinical application [7, 11]. Besides, many coatings have been employed to improve the corrosion resistance of magnesium and its alloys [2, 12]. Given the premise that the coating material is non-toxic, bioactive and the coating is biodegradable, it not only restricts the degradation of the magnesium based materials, but also improves the biocompatibility of the coated system. Such coatings include phosphate chemical conversion

coating [13], plasma electrolytic oxidation coating [14], sol-gel coating [15], and various other approaches.

Among these coating systems, the super-hydrophobic coating is a promising biomimetic coating. Super-hydrophobic coatings have attracted much attention because of their unique properties, including self-cleaning, anti-icing, anti-fogging, resistance to corrosion and mechanical robustness. The super-hydrophobicity of the coating is due to the combination of the rough micro/nanostructure and the low surface energy. Super-hydrophobic coatings have a wide range of application in areas such as multifunctional coatings on transmission lines, eyeglasses, self-cleaning windows, anti-fogging and antireflection optical devices, underwater structures, ships' hulls and corrosion prevention in various industrial processes [16-20]. Particularly, a super-hydrophobic coating can greatly reduce the degradation rate of magnesium and magnesium alloys because the hierarchical micro/nanostructure on the coating surface can trap air [21-23]. Furthermore, the air trapped on the coating surface can block the path of water and aggressive ions to penetrate into the coating. The higher corrosion resistance of the super-hydrophobic coating on magnesium alloys has been reported in many previous studies [24-32]. However, some toxic chemicals, such as fluoroalkylsilane (FAS, $(CF_3(CF_2)_7CH_2CH_2Si(OCH_3)_3)$), are employed in the fabrication process of the hydrophobic/super-hydrophobic coating to reduce the surface energy [31-33].

Many researches have studied the hydrophobic/super-hydrophobic coatings in the biomedical field [34-39]. Machado et al. [35] prepared different substrates with different properties of hydrophobicity/hydrophilicity to compare the properties of cell adhesion. It was indicated that oxygen plasma treatment and high density of vertically aligned carbon nanotube scaffolds (VACNTs) were superior to allow cell adhesion. Compared to hydrophobic surfaces, hydrophilic surface seemed to facilitate cell adhesion. Hung et al. [36] indicated that the hydrophobic rutile TiO_2 film with the nanoporous structure prepared using oxygen plasma

immersion ion implantation (oxygen PIII) was good to improve the blood compatibility. In addition, some studies also investigated the hemocompatibility, cytotoxicity and bacterial adhesion of the super-hydrophobic coatings on magnesium alloys [40, 41]. Wan et al. [40] studied the hemocompatibility of stearic acid based super-hydrophobic coating on AZ31, and the results showed that this coating could inhibit blood platelet adhesion, implying good hemocompatibility. Wang et al. [41] focussed on bacterial adhesion on magnesium hydroxide and stearic acid based super-hydrophobic coating on AZ91D magnesium alloy. The results showed that the coating can obviously restrict the adhesion of the bacteria on magnesium alloy.

In the previous study a calcium stearate based hydrophobic coating on AZ21 magnesium alloy by electrodeposition method was fabricated [42]. The results show that the deposition time and the working voltage have a significant effect on the formation and corrosion resistance of the coating. After parameter optimization the highest corrosion resistance was obtained on the coating fabricated at 50 V for 60 min [42]. The formation mechanism and corrosion mechanism of the coating have been investigated in detail [42]. In addition, influence of surface pre-treatment on the deposition and corrosion properties of this hydrophobic coating has been studied [43]. The results indicate that hydrophobic coating with pre-treatment based on plasma electrolytic oxidation shows the best corrosion resistance in a simulated body fluid [43]. Unfortunately, there are few studies about the influence of this calcium stearate based coating on bone formation. The influence of surface wettability and/or structure on osteoblast adhesion and differentiation is controversially discussed [44]. Moreover, the studied Mg-based alloys contain aluminium (Al) because the addition significantly enhances the mechanical properties by precipitation strengthening effect. However, the Al ions may induce neurotoxicity in the human body [45]. The association of Al with Alzheimer's disease is still under discussion [11].

In this study, pure magnesium was selected as a substrate in order to avoid the negative effects of the Al element. A super-hydrophobic coating was prepared on the pure magnesium with a plasma electrolytic oxidation (PEO) pre-treatment. The cytocompatibility and degradation resistance of all states were analysed in terms of cell adhesion and osteoblast differentiation.

2. Experimental

2.1 Materials and specimen preparation

Commercial pure magnesium (chemical composition of the received material determined by a sparc emission spectrometer (Spectrolab 9, Spectro) is shown in Table 1) of 3 mm thickness was cut into samples with dimensions of 15 × 15 mm. The specimens were abraded with SiC emery paper up to 1500 grade, and cleaned with deionized water and pure ethanol separately. Finally, they were dried in air. All chemicals used in the present work were from analytical grade.

2.2 Plasma electrolytic oxidation

The plasma electrolytic oxidation (PEO) process was carried out by using a self-made pulsed direct current (DC) power source (T_{on}:T_{off} = 0.4ms:3.6ms) under constant voltage regime (400 V) for 10 min and a current density limit of 0.25 A/cm^2. During the PEO process, the specimen and a stainless steel tube were used as the anode and cathode, respectively. The electrolyte for the PEO process was composed of sodium phosphate (10 g/L) and potassium hydroxide (1 g/L). Clay particles [46], 5 g/L (Nanofil 116, Rockwood, natural montmorillonite, about 100% bentonite) with an average size of 12 μm were dispersed into the electrolyte. The temperature of the PEO electrolyte was kept at 10 ± 2℃ by a water cooling system. After PEO process, the specimen was etched in diluted phosphoric acid (60g/L H_3PO_4) for 15 s at room temperature.

2.3 Fabrication of the super-hydrophobic coating

The coating was cathodic electrodeposited on the PEO pre-treated magnesium using a two-electrode cell, in which the PEO pre-treated specimen was used as the cathode and a graphite sheet was used as the anode. The electrolyte contained 0.05 mol/L $Ca(NO_3)_2$ and 0.05 mol/L stearic acid in ethanol (≥99.5%) as solvent. The deposition process was performed at 50 V for 60 min using a DC power supply (EA-PS 8720-15, Elektro-Automatik GmbH) in voltage control mode at room temperature. After electrodeposition, the coated specimens were cleaned with ethanol and dried in air. The current density vs. time (*J-t*) curve was recorded within the first 900 s of the coating preparation.

The specimen coated with the super-hydrophobic coating was named PEO-SHC and the plasma electrolytic oxidation pre-treated specimen was named PEO.

2.4 Characterization of the super-hydrophobic coating

The surface morphology of the PEO pre-treated layer and the coating along with the cross-sectional morphology of the coating were examined using a Tescan Vega3 SB scanning electron microscopy (SEM) equipped with an energy dispersive spectrometer (EDS, Iridium Ultra from Eumex). Phase compositions were examined by X-ray diffraction (XRD), with a Bruker D5000 X-ray diffractometer using a Cu Kα radiation source at 40 kV and 40 mA. The data collection was performed by 2θ scan method at a scan speed of 0.01°/s from 20° to 80°. Static water contact angles were measured with contact angle measuring system (Dataphysics OCA20, Germany) at ambient temperature. The volume of deionized water droplets used in the measurement was 3 μL. In order to obtain a reliable result, the value of the static water contact angle was recorded after the water droplet stayed for 1 min on the surface of the coating and the contact angles were measured three times for each specimen.

2.5 Electrochemical measurements

Electrochemical tests were performed in Kokubo's Simulated Body Fluid (SBF) at 37 ± 0.5 ℃ using a Gamry (Reference 600) computer-controlled potentiostat. The SBF contained

8.035 g/L NaCl, 0.355 g/L $NaHCO_3$, 0.225 g/L KCl, 0.231 g/L $K_2HPO_4 \cdot 3H_2O$, 0.311 g/L $MgCl_2 \cdot 6H_2O$, 0.292 g/L $CaCl_2$ and 0.072 g/L Na_2SO_4 [47]. The pH of the SBF was adjusted to 7.4 with 1 mol/L HCl and tris (hydroxymethyl) aminomethane ($(CH_2OH)_3CNH_2$). All tests were measured in a three-electrode cell with a saturated calomel reference electrode (SCE) and a platinum counter electrode. The specimen was used as working electrode with an exposed surface area of 1 cm^2. For potentiodynamic polarization curves, the open circuit potential (OCP) was set to stabilize for 30 min and the scanning rate was set to 0.5 mV/s. Electrochemical impedance spectroscopy (EIS) measurements were performed by applying a sinusoidal potential perturbation of 10 mV RMS (at OCP) and a frequency sweep from 10^5 Hz to 10^{-2} Hz. All electrochemical tests were repeated three times with good reproducibility. EIS results were analyzed by fitting data with ZSimpWin software.

2.6 Characterization of degradation

The degradation behaviour of the bare magnesium and the PEO and PEO-SHC samples (each n=4) was analysed by immersion in a semi-static system for 10 days under physiological conditions (37 °C, 5 % CO_2, 20 % O_2, 95 % relative humidity). As immersion medium 6 mL of Dulbecco's modified eagle medium (DMEM GlutaMAX, Life Technologies, Darmstadt, Germany) with the addition of 10 % fetal bovine serum (FBS, PAA Laboratories, Linz, Austria) was used. The starting pH value of the medium is 7.6. And the medium was changed every 2-3 days. Due to the fact that the determination of degradation rate by the use of chromic acid is not applicable for coated samples, an indirect determination by assessing the osmolality and pH-value was used. Osmolality was measured at each medium change by a freezing point osmometer (Osmomat 030, Gonotec, Berlin, Germany), as well as the pH-value (Sentron Argus X pH-meter, Fisher Scientific GmbH, Schwerte, Germany).

2.7 Cell experiments and stainings

The isolation of primary human osteoblasts was performed according to the Declaration of Helsinki. Human hip joints were obtained from patients undergoing hip arthroplasty (Schön Klinik Hamburg Eilbek, Hamburg, Germany) with the approval of the local ethic committee (Board of medical doctors, Hamburg, Germany). Cancellous bone was removed from the hip joint bone and transferred to a cell culture flask according to the protocol of Gallagher [48]. Then cancellous particles were covered with cell culture medium (DMEM Glutamax + 10 % FBS) and incubated until around 90% confluent growth was reached. For this study osteoblasts were used up to the third passage. On each sample 100.000 osteoblasts were cultivated and analysed after 7, 14 and 21 days.

For the assessment of osteoblast cell coverage and viability the Live/Dead assay (Life Technologies, Darmstadt, Germany) was used after each immersion time point. The staining solution was prepared by adding 4 µl Calcein AM (Live) and 10 µl Ethidium homodimer-1 (Dead) to 10 mL of phosphate buffered saline (PBS). The samples were washed with sterile distilled water to eliminate the non-adherent cells, followed by immersing each sample with 1.5 mL of staining solution and incubation under a 5% CO_2 atmosphere at 37 °C for 20 minutes. Afterwards the staining solution was replaced by DMEM and samples were visualized by a fluorescent microscope (Nikon,Eclipse Ti, Düsseldorf, Germany). The applied filters were Fluorescence Isothiocynate; FITC (Ex: 465-495 nm; Em: 515-555 nm; Mirror at 505 nm) and Texas red (Ex: 540-580nm; Em: 600-660; Mirror at 595 nm).

Osteo-Image (Lonza, Walkersville, USA) was used as a specific staining for hydroxyapatite (HA). Samples were removed from the incubator and allowed to reach room temperature (RT). The medium was removed and discs were washed once with sterile water. The samples were subsequently fixed with 3.7 % formaldehyde in water (Sigma-Aldrich, Taufkirchen, Germany) at RT for 20 minutes and then washed twice with Osteo-Image wash

buffer (diluted 1:10 in deionized water). 1 mL of the staining reagent (diluted 1:100 in staining reagent dilution buffer) was added to each sample, and the mixture was incubated at RT for 30 minutes protected from light. The staining reagent was removed, and the samples were washed three times with washing buffer. The samples were analysed under a fluorescence microscope with a FITC filter.

2.8 Statistical analysis

Statistics were performed using the SigmaStat package (Systat software GmbH, Erkrath, Germany). Prior to statistical analysis the data were checked for normal distribution (Shapiro–Wilk-test) and for equal variance. Analysis comparing more than two treatments was then done according to the test result. If normal distribution and equal variance were fulfilled a one-way analysis of variance (ANOVA) with Holm-Sidak post hoc test was performed. In the other cases statistical analysis was done by using ANOVA on ranks with Dunn's multiple comparison post hoc test. Statistical values are indicated at the relevant experiments.

3. Results and discussion

Fig. 1 shows the XRD diffraction patterns of the PEO substrate with and without the super-hydrophobic coating. On the PEO substrate the main diffraction peaks were determined as MgO, whereas on the super-hydrophobic coating the main diffraction peak was identified as calcium stearate. Apart from this, the peaks of Mg can be found on both the PEO substrate and the coated sample.

EDS was applied to determine the elemental composition of the magnesium, the PEO and PEO-SHC (as shown in Table 2). Compared with bare magnesium, phosphate, sodium and potassium appear in the PEO layer, which is related to the sodium phosphate and potassium hydroxide in the electrolyte. The appearance of silicon, calcium and iron might be

due to the clay particles in the electrolyte. Carbon, oxygen and calcium appear in the super-hydrophobic coating, which is consistent with the XRD results (as shown in Fig. 1).

The surface morphologies of the PEO substrate and the super-hydrophobic coating are shown in Fig. 2. The static water contact angles on these surfaces are shown in the insets, respectively. SEM image (Fig. 2a) reveals that the surface of the PEO substrate is dominated by numerous pores which are characteristic of PEO coating. In particular, some of the pores are sealed. The static water contact angle on the surface of the PEO substrate is 46.0 °, indicating that the PEO surface shows hydrophilicity. SEM images of the super-hydrophobic coating (Fig. 2b) reveal a micro/nanostructure on the surface. The surface is composed of protrusions with an average diameter of about 30 μm, the nanostructure is observed on the surface of the protrusion (the inset in Fig. 2b). The static water contact angle on the coating surface is 150.9 °, indicating that the coating exhibits super-hydrophobic behavior. The micro/nanostructure on the coating surface is responsible for the super-hydrophobicity. The cross-sectional image of the coated sample is shown in Fig. 2c. The super-hydrophobic coating and the PEO pre-treated layer can be seen clearly. The thickness of the PEO layer and the super-hydrophobic coating is about 12 μm and 23 μm, respectively.

The polarization curves of the magnesium, the PEO substrate and the PEO-SHC are depicted in Fig. 3. The corrosion potential (E_{corr}), corrosion current density (i_{corr}) and breakdown potential (E_{bd}) derived from Fig. 3 are shown in Table 3. Compared to Mg, an obvious passivation region exists on the curves of PEO and PEO-SHC. This implies that the pre-treatment with and without the coating can improve the degradation protection properties of magnesium, in which the super-hydrophobic coating provides a more effective protection for the substrate. The corrosion current density of the PEO-SHC is 3 orders of magnitude lower than that of the PEO. The E_{bd} of the sample PEO-SHC is -1.32 ± 0.02 V (vs. SCE), which is more positive than that of the PEO (-1.57 ± 0.01 V (vs. SCE)).

Fig. 4 depicts the electrochemical impedance spectra of the PEO-SHC, immersed in SBF for the different times. The symbols are the experimental data and the solid lines are fitting data. Just after immersion the impedance modulus (Fig. 4a) shows a relatively high value over the whole frequency range (0 h of immersion), which indicates the higher barrier properties of the combination of the super-hydrophobic coating and the PEO layer. With increasing immersion time, the impedance modulus decreases gradually. Obvious drops of the modulus are mainly observed from 0 h to 1 h and 24 h to 48 h. Two time constants (Fig. 4b) are observed from the phase angle vs. frequency curves at 0 h and 1 h of immersion. The time constant at high frequency is related to the super-hydrophobic coating and the other one at the middle frequency is due to the PEO layer. From 6 h to 120 h, a new time constant appears at the low frequency (at around 1 Hz), which can be ascribed to the electrochemical processes at the magnesium/SBF interface.

The equivalent circuit model in Fig. 5a is used to fit the EIS data obtained at 0 h and 1 h of immersion. The model in Fig. 5b is used to fit the EIS data from 6 h to 120 h. In these circuits, R_s is the solution resistance, CPE_{coat} and R_{coat} represent the capacitance and resistance of the super-hydrophobic coating, CPE_{PEO} and R_{PEO} represent the capacitance and resistance of the PEO layer, CPE_{dl} stands for the electrochemical double layer capacitance and R_{ct} is the charge transfer resistance.

The resistance values obtained from the EIS fitting results of the PEO-SHC are presented in Fig. 6. The R_{coat} value drops significantly within the first hour of immersion, which is related to water and aggressive ions starting to penetrate the coating. Afterwards it stabilizes until 24 h. Subsequently another great drop is clearly visible, followed by stabilization around 3×10^3 $\Omega\cdot cm^2$. The decrease between 24 h and 48 h indicates the failure of the barrier property of the super-hydrophobic coating. The PEO layer without the super-hydrophobic coating demonstrated lower degradation resistance in SBF (Fig.3). With the presence of the top

coating (R_{coat}), the R_{PEO} shows a much higher and relative stable value within the immersion period. Although, the R_{PEO} values also display a downward trend during the immersion process, it can stabilizes at approximately 4×10^4 $\Omega\cdot cm^2$ after 48 h of immersion. Thus, the super-hydrophobic coating is still able to protect the oxide layer by preventing direct contact of the PEO layer with electrolyte and the R_{PEO} value decreases slowly and then remains stable. As a consequence, the oxide layer, together with the super-hydrophobic coating, generates a high degradation resistance, which protects the underlying magnesium bulk. This contributes to the high R_{ct} value of approximately 1×10^6 $\Omega\cdot cm^2$ during the full immersion period.

The degradation properties in physiological environment were analyzed by the determination of pH and osmolality (Fig. 7). The pH-value evolution shows general differences between the uncoated and coated specimen. The uncoated specimen shows an initially high pH, followed by a lower plateau and a dramatic increase from 7-10 days. In contrast, both coated specimens show similar behavior, showing a linear increase until day 7 and then a stabilisation. However, the pH-values for the PEO-SHC are generally lower. In analyzing the osmolality values this trend is more obvious. Uncoated specimen shows a typical high initial osmolality and afterwards a linear behavior, which is lower on PEO and PEO-SHC. At the latter specimen the difference to the uncoated samples is statistically significant for all time points (ANOVA with Holm-Sidak post-hoc test). This behavior is consistent with the electrochemical measurements, showing a higher degradation resistance of both coatings also under physiological conditions, with PEO-SHC being the most protective.

Cell adhesion and differentiation were followed over 21 days. It can be observed, that on the uncoated specimen after 7 days only few cells are visible. The cell number increases at the later time points and the formation of hydroxyapatite (HA) can be observed after 14 days. These results are comparable to another study on different alloys [3]. A thin layer of HA is formed on the PEO samples after 7 days, and over time the amount of cells on the samples

increases dramatically, leading to a full cell coverage after 21 days (Fig. 8). The formed hydroxyapatite can only be observed locally in higher amounts. This coating seems to exhibit a proliferative effect. The super-hydrophobic coating leads to a completely different behavior. Cell coverage on all time points is much lower compared to the other samples. However, the cells begin very early to differentiate in a nodule-like morphology. This is already observable after 7 days and increases until day 21.

This behavior is somewhat unexpected, as it is hypothesized that the super-hydrophobic coating would behave as anti-adhesive and degradation protective surface. While the degradation protective effect can be confirmed by electrochemical measurements and immersion tests, osteoblasts in contact with the surface react with spontaneous, nodule-like differentiation pattern. A similar behavior of mesenchymal stem cells was observed on very hydrophilic surfaces [49]. Several other studies confirmed this behavior for osteoblasts on a variety of superhydrophilic surfaces made of different materials (e.g. [50, 51]). The preferential adhesion of rat osteoblasts to surfaces like titanium or hydroxyapatite is explained by the hydrophilic character of osteoblast cell layers [52]. On such surfaces like titanium the advancing contact angle is in average between 70 and 80 ° [53], so much lower than obtained in this study. Studies with osteoblasts on super-hydrophobic surfaces are sparse. For example, on super-hydrophobic copper nanowire arrays the adhesion of osteoblasts was enhanced [54], but no focus was laid on differentiation, i.e. the formation of hydroxyapatite. For super-hydrophobic aluminum a reduction of protein and bacterial adhesion could be observed, but no cell adhesion experiments were performed [55]. A comparable cell behavior consisting of low cell adhesion and enhanced differentiation of MC3T3-E1 mouse osteoblastic cell line and primary bovine articular chondrocytes was observed on polymeric super-hydrophobic surfaces (polystyrene and poly(L-lactid acid)) [56]. A super-hydrophobically modified Polytetrafluoroethylene (PTFE) surface also exhibited the strongest effect on differentiation

of rat calvarial osteoblasts [57]. Moreover, calcium stearate was reported to promote osteogenic differentiation and mineralization of osteoblasts and vascular smooth muscle cells [58]. Therefore, the assumption that a combinatorial effect of physical and biochemical clues are responsible for the early onset of osteoblast differentiation on the super-hydrophobic coating, seems to be valid. In further studies the adhesion of proteins on this surface, as well as the formation of focal adhesions during osteoblast attachment should be analysed.

4. Conclusions

A super-hydrophobic coating was prepared on the surface of PEO pre-treated pure magnesium by cathodic electrodeposition. The corrosion behaviour and corrosion mechanism of the PEO-SHC were investigated. And the cytocompatibility was studied as well. The following conclusion can be drawn:

(1) A super-hydrophobic coating with a hierarchical micro/nanostructure surface is formed on the surface of the PEO coated substrate. The coating is composed of calcium stearate.

(2) EIS clarifies the change of the corrosion mechanism of the PEO-SHC. Bode plots evolve from two time constants to three time constants. Two time constants are distributed at high and medium frequency zones before 1 h of immersion. They are related to the super-hydrophobic coating and the PEO pre-treated layer, respectively. A new time constant at low frequency appears after 6 h of immersion, which is the electrochemical double layer at the magnesium/SBF interface.

(3) The super-hydrophobic coating decreases the substrate corrosion. The resistance of coating itself is approximately 3×10^3 $\Omega\cdot cm^2$, but it is able to effectively protect the oxide layer. The PEO layer functions as a main protective layer, and prevents the corrosion of the magnesium in SBF and also under physiological conditions.

(4) As the super-hydrophobic coating increases the differentiation of osteoblasts, it could be an interesting material for bone applications, in which fast bone bonding is necessary.

Acknowledgments

The authors want to acknowledge G. Salamon for expert technical assistance. The Project was supported by the National Natural Science Foundation of China (Grant no. 51272055 and 51501050). Yufen Zhang thanks China Scholarship Council for the award of fellowship and funding. Frank Feyerabend has received funding from the Helmholtz Virtual Institute "In vivo studies of biodegradable magnesium based implant materials (MetBioMat)" under grant agreement n° VH-VI-523.

References

[1] H. Yang, K. Xia, T. Wang, J. Niu, Y. Song, Z. Xiong, K. Zheng, S. Wei, W. Lu, Growth, in vitro biodegradation and cytocompatibility properties of nano-hydroxyapatite coatings on biodegradable magnesium alloys, J. Alloys Compd. 672 (2016) 366-373.

[2] S. Gaur, R.K. Singh Raman, A.S. Khanna, In vitro investigation of biodegradable polymeric coating for corrosion resistance of Mg-6Zn-Ca alloy in simulated body fluid, Mater. Sci. Eng. C, Mater. Biol. Appl. 42 (2014) 91-101.

[3] N. Ahmad Agha, R. Willumeit-Romer, D. Laipple, B. Luthringer, F. Feyerabend, The Degradation Interface of Magnesium Based Alloys in Direct Contact with Human Primary Osteoblast Cells, PloS one, 11 (2016) e0157874.

[4] Y. Zhang, J. Xu, Y.C. Ruan, M.K. Yu, M. O'Laughlin, H. Wise, D. Chen, L. Tian, D. Shi, J. Wang, S. Chen, J.Q. Feng, D.H.K. Chow, X. Xie, L. Zheng, L. Huang, S. Huang, K. Leung, N. Lu, L. Zhao, H. Li, D. Zhao, X. Guo, K. Chan, F. Witte, H.C. Chan, Y. Zheng, L. Qin, Implant-derived magnesium induces local neuronal production of CGRP to improve bone-fracture healing in rats, Nat Med, advance online publication (2016).

[5] D. Xue, Y. Yun, M.J. Schulz, V. Shanov, Corrosion protection of biodegradable magnesium implants using anodization, Mater. Sci. Eng. C, Mater. Biol. Appl. 31 (2011) 215-223.

[6] W.F. Ng, K.Y. Chiu, F.T. Cheng, Effect of pH on the in vitro corrosion rate of magnesium degradable implant material, Mater. Sci. Eng. C, Mater. Biol. Appl. 30 (2010) 898-903.

[7] X. Lin, L. Tan, Q. Wang, G. Zhang, B. Zhang, K. Yang, In vivo degradation and tissue compatibility of ZK60 magnesium alloy with micro-arc oxidation coating in a transcortical model, Mater. Sci. Eng. C, Mater. Biol. Appl. 33 (2013) 3881-3888.

[8] W. He, E. Zhang, K. Yang, Effect of Y on the bio-corrosion behavior of extruded Mg–Zn–Mn alloy in Hank's solution, Mater. Sci. Eng. C, Mater. Biol. Appl. 30 (2010) 167-174.

[9] P. Saha, M. Roy, M.K. Datta, B. Lee, P.N. Kumta, Effects of grain refinement on the biocorrosion and in vitro bioactivity of magnesium, Mater. Sci. Eng. C, Mater. Biol. Appl. 57 (2015) 294-303.

[10] B. Ratna Sunil, T.S. Sampath Kumar, U. Chakkingal, V. Nandakumar, M. Doble, V. Devi Prasad, M. Raghunath, In vitro and in vivo studies of biodegradable fine grained AZ31 magnesium alloy produced by equal channel angular pressing, Mater. Sci. Eng. C, Mater. Biol. Appl. 59 (2016) 356-367.

[11] C. Zhao, F. Pan, L. Zhang, H. Pan, K. Song, A. Tang, Microstructure, mechanical properties, bio-corrosion properties and cytotoxicity of as-extruded Mg-Sr alloys, Mater. Sci. Eng. C, Mater. Biol. Appl. 70 (2017) 1081-1088.

[12] M. Razavi, M. Fathi, O. Savabi, D. Vashaee, L. Tayebi, In vivo assessments of bioabsorbable AZ91 magnesium implants coated with nanostructured fluoridated hydroxyapatite by MAO/EPD technique for biomedical applications, Mater. Sci. Eng. C, Mater. Biol. Appl. 48 (2015) 21-27.

[13] B. Liu, X. Zhang, G.Y. Xiao, Y.P. Lu, Phosphate chemical conversion coatings on metallic substrates for biomedical application: a review, Mater. Sci. Eng. C, Mater. Biol. Appl. 47 (2015) 97-104.

[14] Y. Jang, Z. Tan, C. Jurey, B. Collins, A. Badve, Z. Dong, C. Park, C.S. Kim, J. Sankar, Y. Yun, Systematic understanding of corrosion behavior of plasma electrolytic oxidation treated AZ31 magnesium alloy using a mouse model of subcutaneous implant, Mater. Sci. Eng. C, Mater. Biol. Appl. 45 (2014) 45-55.

[15] S. Agarwal, J. Curtin, B. Duffy, S. Jaiswal, Biodegradable magnesium alloys for orthopaedic applications: A review on corrosion, biocompatibility and surface modifications, Mater. Sci. Eng. C, Mater. Biol. Appl. 68 (2016) 948-963.

[16] Z. She, Q. Li, Z. Wang, C. Tan, J. Zhou, L. Li, Highly anticorrosion, self-cleaning superhydrophobic Ni–Co surface fabricated on AZ91D magnesium alloy, Surf. Coat. Technol. 251 (2014) 7-14.

[17] Q. Liu, Z. Kang, One-step electrodeposition process to fabricate superhydrophobic surface with improved anticorrosion property on magnesium alloy, Mater. Lett. 137 (2014) 210-213.

[18] Z. Zuo, R. Liao, C. Guo, Y. Yuan, X. Zhao, A. Zhuang, Y. Zhang, Fabrication and anti-icing property of coral-like superhydrophobic aluminum surface, Appl. Surf. Sci. 331 (2015) 132-139.

[19] A.M.A. Mohamed, A.M. Abdullah, N.A. Younan, Corrosion behavior of superhydrophobic surfaces: A review, Arab. J. Chem. 8 (2015) 749-765.

[20] Q. Shang, Y. Zhou, Fabrication of transparent superhydrophobic porous silica coating for self-cleaning and anti-fogging, Ceram. Int. 42 (2016) 8706-8712.

[21] J. Zhang, Z. Kang, Effect of different liquid–solid contact models on the corrosion resistance of superhydrophobic magnesium surfaces, Corros. Sci. 87 (2014) 452-459.

[22] L. Zhao, Q. Liu, R. Gao, J. Wang, W. Yang, L. Liu, One-step method for the fabrication of superhydrophobic surface on magnesium alloy and its corrosion protection, antifouling performance, Corros. Sci. 80 (2014) 177-183.

[23] T. Ishizaki, Y. Masuda, M. Sakamoto, Corrosion resistance and durability of superhydrophobic surface formed on magnesium alloy coated with nanostructured cerium oxide film and fluoroalkylsilane molecules in corrosive NaCl aqueous solution, Langmuir 27 (2011) 4780-4788.

[24] T. Ishizaki, J. Hieda, N. Saito, N. Saito, O. Takai, Corrosion resistance and chemical stability of super-hydrophobic film deposited on magnesium alloy AZ31 by microwave plasma-enhanced chemical vapor deposition, Electrochim. Acta 55 (2010) 7094-7101.

[25] Y. Liu, X. Yin, J. Zhang, S. Yu, Z. Han, L. Ren, A electro-deposition process for fabrication of biomimetic super-hydrophobic surface and its corrosion resistance on magnesium alloy, Electrochim. Acta 125 (2014) 395-403.

[26] X.-j. Cui, X.-z. Lin, C.-h. Liu, R.-s. Yang, X.-w. Zheng, M. Gong, Fabrication and corrosion resistance of a hydrophobic micro-arc oxidation coating on AZ31 Mg alloy, Corros. Sci. 90 (2015) 402-412.

[27] J. Wang, D. Li, Q. Liu, X. Yin, Y. Zhang, X. Jing, M. Zhang, Fabrication of hydrophobic surface with hierarchical structure on Mg alloy and its corrosion resistance, Electrochim. Acta 55 (2010) 6897-6906.

[28] D. Zang, R. Zhu, C. Wu, X. Yu, Y. Zhang, Fabrication of stable superhydrophobic surface with improved anticorrosion property on magnesium alloy, Scr. Mater. 69 (2013) 614-617.

[29] T. Ishizaki, M. Sakamoto, Facile formation of biomimetic color-tuned superhydrophobic magnesium alloy with corrosion resistance, Langmuir 27 (2011) 2375-2381.

[30] Z. Wang, Q. Li, Z. She, F. Chen, L. Li, Low-cost and large-scale fabrication method for an environmentally-friendly superhydrophobic coating on magnesium alloy, J. Mater. Chem. 22 (2012) 4097.

[31] W. Xu, J. Song, J. Sun, Y. Lu, Z. Yu, Rapid fabrication of large-area, corrosion-resistant superhydrophobic Mg alloy surfaces, ACS Appl. Mater. & interfaces 3 (2011) 4404-4414.

[32] T. Ishizaki, N. Saito, Rapid formation of a superhydrophobic surface on a magnesium alloy coated with a cerium oxide film by a simple immersion process at room temperature and its chemical stability, Langmuir 26 (2010) 9749-9755.

[33] J. Wang, D. Li, R. Gao, Q. Liu, X. Jing, Y. Wang, Y. He, M. Zhang, Z. Jiang, Construction of superhydrophobic hydromagnesite films on the Mg alloy, Mater. Chem. Phys. 129 (2011) 154-160.

[34] S. Zangi, I. Hejazi, J. Seyfi, E. Hejazi, H.A. Khonakdar, S.M. Davachi, Tuning cell adhesion on polymeric and nanocomposite surfaces: Role of topography versus superhydrophobicity, Mater. Sci. Eng. C, Mater. Biol. Appl. 63 (2016) 609-615.

[35] M.M. Machado, A.O. Lobo, F.R. Marciano, E.J. Corat, M.A.F. Corat, Analysis of cellular adhesion on superhydrophobic and superhydrophilic vertically aligned carbon nanotube scaffolds, Mater. Sci. Eng. C, Mater. Biol. Appl. 48 (2015) 365-371.

[36] W.C. Hung, F.M. Chang, T.S. Yang, K.L. Ou, C.T. Lin, P.W. Peng, Oxygen-implanted induced formation of oxide layer enhances blood compatibility on titanium for biomedical applications, Mater. Sci. Eng. C, Mater. Biol. Appl. 68 (2016) 523-529.

[37] H.S. Salapare, 3rd, B.A. Suarez, H.S. Cosinero, M.Y. Bacaoco, H.J. Ramos, Irradiation of poly(tetrafluoroethylene) surfaces by CF4 plasma to achieve robust superhydrophobic and enhanced oleophilic properties for biological applications, Mater. Sci. Eng. C, Mater. Biol. Appl. 46 (2015) 270-275.

[38] A. Díaz, L.J. del Valle, D. Tugushi, R. Katsarava, J. Puiggalí, New poly(ester urea) derived from l-leucine: Electrospun scaffolds loaded with antibacterial drugs and enzymes, Mater. Sci. Eng. C, Mater. Biol. Appl. 46 (2015) 450-462.

[39] E. Llorens, S. Calderon, L.J. del Valle, J. Puiggali, Polybiguanide (PHMB) loaded in PLA scaffolds displaying high hydrophobic, biocompatibility and antibacterial properties, Mater. Sci. Eng. C, Mater. Biol. Appl. 50 (2015) 74-84.

[40] P. Wan, J. Wu, L. Tan, B. Zhang, K. Yang, Research on super-hydrophobic surface of biodegradable magnesium alloys used for vascular stents, Mater. Sci. Eng. C, Mater. Biol. Appl. 33 (2013) 2885-2890.

[41] Z. Wang, Y. Su, Q. Li, Y. Liu, Z. She, F. Chen, L. Li, X. Zhang, P. Zhang, Researching a highly anti-corrosion superhydrophobic film fabricated on AZ91D magnesium alloy and its anti-bacteria adhesion effect, Mater. Charact. 99 (2015) 200-209.

[42] Y. Zhang, S. Tang, J. Hu, T. Lin, Formation mechanism and corrosion resistance of the hydrophobic coating on anodized magnesium, Corros. Sci. 111 (2016) 334-343.

[43] Y. Zhang, C. Blawert, S. Tang, J. Hu, M. Mohedano, M.L. Zheludkevich, K.U. Kainer, Influence of surface pre-treatment on the deposition and corrosion properties of hydrophobic coatings on a magnesium alloy, Corros. Sci. 112 (2016) 483-494.

[44] M.M. Gentleman, E. Gentleman, The role of surface free energy in osteoblast–biomaterial interactions, Int. Mater. Rev. 59 (2014) 417-429.

[45] C.A. Shaw, M.S. Petrik, Aluminum hydroxide injections lead to motor deficits and motor neuron degeneration, J. Inorg. Biochem. 103 (2009) 1555-1562.

[46] X. Lu, S.P. Sah, N. Scharnagl, M. Störmer, M. Starykevich, M. Mohedano, C. Blawert, M.L. Zheludkevich, K.U. Kainer, Degradation behavior of PEO coating on AM50 magnesium alloy produced from electrolytes with clay particle addition, Surf. Coat. Technol. 269 (2015) 155-169.

[47] T. Kokubo, H. Takadama, How useful is SBF in predicting in vivo bone bioactivity?, Biomaterials, 27 (2006) 2907-2915.

[48] J.A. Gallagher, Human osteoblast culture, Methods Mol Med, 80 (2003) 3-18.

[49] R. Willumeit, M. Schossig, H. Clemens, F. Feyerabend, In-vitro interactions of human chondrocytes and mesenchymal stem cells, and of mouse macrophages with phospholipid-covered metallic implant materials, Eur. cells & mater. 13 (2007) 11-25.

[50] F. Otsuka, Y. Kataoka, T. Miyazaki, Enhanced osteoblast response to electrical discharge machining surface, Dent. Mater. J. 31 (2012) 309-315.

[51] H. Zhao, W. Dong, Y. Zheng, A. Liu, J. Yao, C. Li, W. Tang, B. Chen, G. Wang, Z. Shi, The structural and biological properties of hydroxyapatite-modified titanate nanowire scaffolds, Biomaterials, 32 (2011) 5837-5846.

[52] P. Zanchetta, J. Guezennec, Surface thermodynamics of osteoblasts: relation between hydrophobicity and bone active biomaterials, Colloids Surf B Biointerfaces, 22 (2001) 301-307.

[53] R. Willumeit, F. Feyerabend, H. Kamusewitz, M. Schossig, H. Clemens, Biological Multi-layer Systems as Implant Surface Modification, Matwiss Werkst, 34 (2003) 1084-1093.

[54] J. Zhou, J.-B. Fan, Q. Nie, S. Wang, Three-dimensional superhydrophobic copper 7,7,8,8-tetracyanoquinodimethane biointerfaces with the capability of high adhesion of osteoblasts, Nanoscale, 8 (2016) 3264-3267.

[55] P. Moazzam, A. Razmjou, M. Golabi, D. Shokri, A. Landarani-Isfahani, Investigating the BSA protein adsorption and bacterial adhesion of Al-alloy surfaces after creating a hierarchical (micro/nano) superhydrophobic structure, J. Biomed. Mater. Res. A, 104 (2016) 2220-2233.

[56] B.N. Lourenço, G. Marchioli, W. Song, R.L. Reis, C.A.v. Blitterswijk, M. Karperien, A.v. Apeldoorn, J.F. Mano, Wettability Influences Cell Behavior on Superhydrophobic Surfaces with Different Topographies, Biointerphases, 7 (2012) 46.

[57] H. Wang, D.T.K. Kwok, W. Wang, Z. Wu, L. Tong, Y. Zhang, P.K. Chu, Osteoblast behavior on polytetrafluoroethylene modified by long pulse, high frequency oxygen plasma immersion ion implantation, Biomaterials, 31 (2010) 413-419.

[58] M. Masuda, T.C. Ting, M. Levi, S.J. Saunders, S. Miyazaki-Anzai, M. Miyazaki, Activating transcription factor 4 regulates stearate-induced vascular calcification, J. Lipid Res. 53 (2012) 1543-1552.

Figure/Table captions

Fig. 1. XRD patterns of the PEO and the PEO-SHC. The main peaks are magnesium (Mg), magnesium oxide (MgO) and calcium stearate ($C_{35}H_{70}CaO_4$).

Fig. 2. Surface morphologies of the PEO coating (a) and the PEO-SHC (b); the inset in (a) is the static contact angle of water droplet on the surface of PEO; the insets in (b) are high magnification image and static contact angle of water droplet on the surface of PEO-SHC. (c) is the cross-sectional image of the PEO-SHC.

Fig. 3. Polarization curves of the bare magnesium, the PEO and PEO-SHC.

Fig. 4. Bode plots evolution of the PEO-SHC for different SBF exposure time at 37 ± 0.5 °C. The symbols are the experimental data and the solid lines are fitting data.

Fig. 5. Electrical equivalent circuits used to fit the EIS diagrams of the PEO-SHC during the different SBF immersion periods at 37 ± 0.5 °C: (a) 0 h and 1 h; (b) 6 h–120 h. R_s is the solution resistance, CPE_{coat} and R_{coat} represent the capacitance and resistance of the super-hydrophobic coating, CPE_{PEO} and R_{PEO} represent the capacitance and resistance of the PEO layer, CPE_{dl} stands for the electrochemical double layer capacitance and R_{ct} is the charge transfer resistance.

Fig. 6. The evolution of resistance values (obtained from EIS fitting results) with immersion in SBF at 37 ± 0.5 °C for the PEO-SHC.

Fig. 7. pH (left) and osmolality measurements (right) performed at each medium change (Days 3, 5, 7 and 10). The asterisks indicate significant differences of the PEO-SHC to the uncoated specimen ($p<0.05$). Statistical analysis was done with ANOVA with Holm-Sidak post-hoc test.

Fig 8. Live/dead staining and determination of hydroxyapatite by Osteoimage (green) on the different samples, observed by fluorescence microscopy. White scale bars = 100 μm, black scale bar = 2000 μm.

Table 1 Chemical composition of the as received material.

Table 2 Surface element composition of the bare magnesium, the PEO and PEO-SHC determined by EDS analysis.

Table 3 Electrochemical data of the samples as read from Fig. 3.

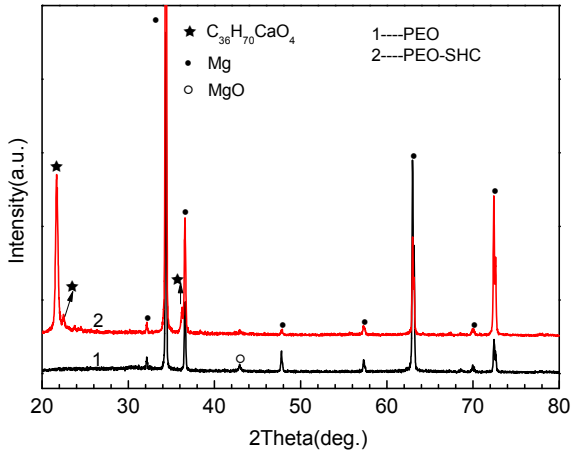

Fig. 1. XRD patterns of the PEO and the PEO-SHC. The main peaks are magnesium (Mg), magnesium oxide (MgO) and calcium stearate ($C_{35}H_{70}CaO_4$).

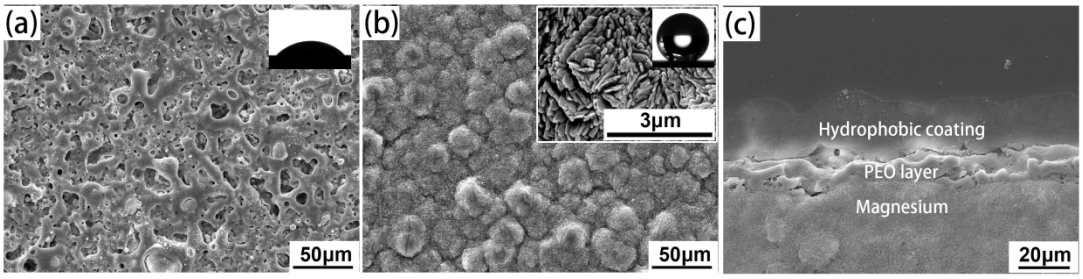

Fig. 2. Surface morphologies of the PEO coating (a) and the PEO-SHC (b); the inset in (a) is the static contact angle of water droplet on the surface of PEO; the insets in (b) are high magnification image and static contact angle of water droplet on the surface of PEO-SHC. (c) is the cross-sectional image of the PEO-SHC.

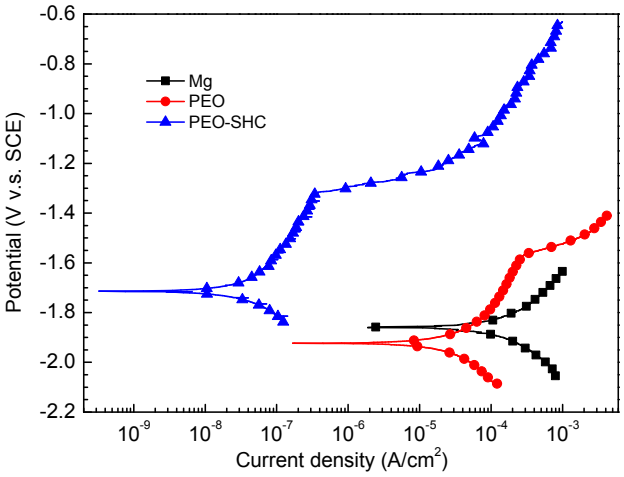

Fig. 3. Polarization curves of the bare magnesium, the PEO and PEO-SHC.

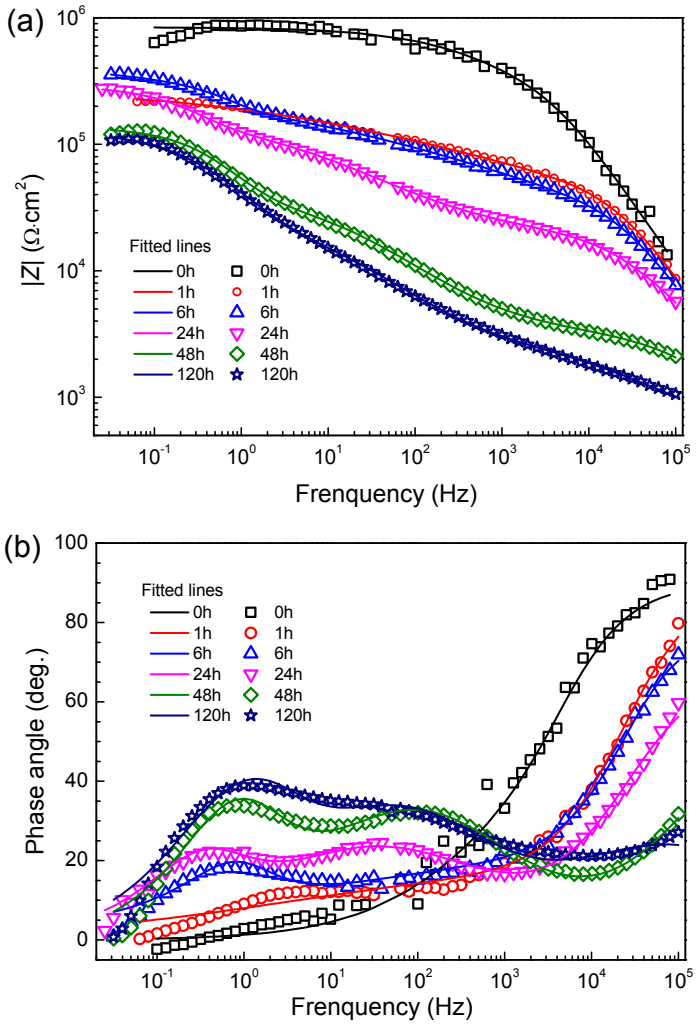

Fig. 4. Bode plots evolution of the PEO-SHC for different SBF exposure time at 37 ± 0.5 °C. The symbols are the experimental data and the solid lines are fitting data.

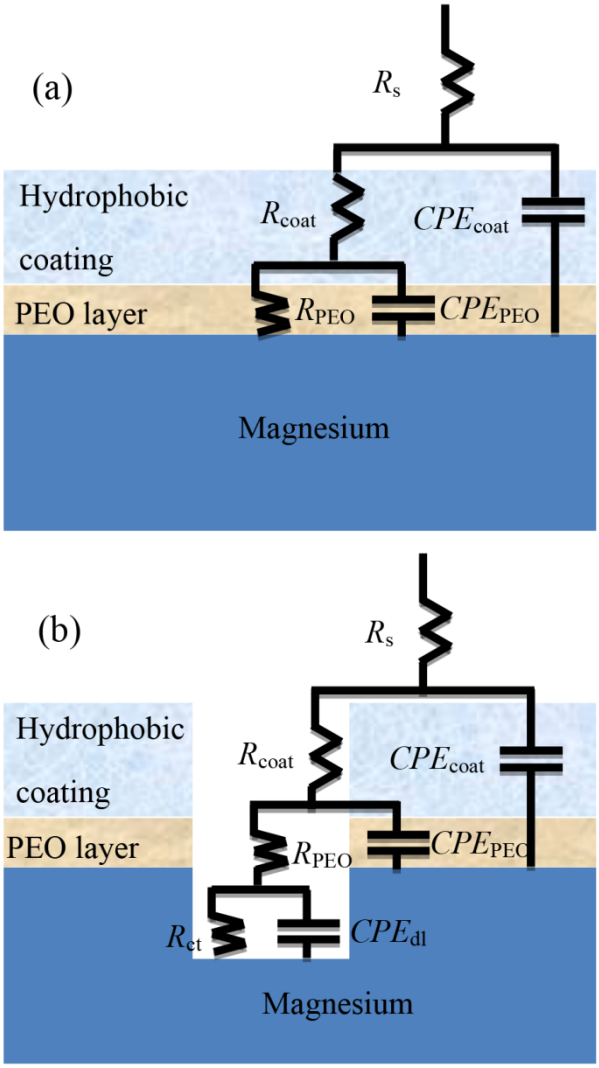

Fig. 5. Electrical equivalent circuits used to fit the EIS diagrams of the PEO-SHC during the different SBF immersion periods at 37 ± 0.5 °C: (a) 0 h and 1 h; (b) 6 h–120 h. R_s is the solution resistance, CPE_{coat} and R_{coat} represent the capacitance and resistance of the super-hydrophobic coating, CPE_{PEO} and R_{PEO} represent the capacitance and resistance of the PEO layer, CPE_{dl} stands for the electrochemical double layer capacitance and R_{ct} is the charge transfer resistance.

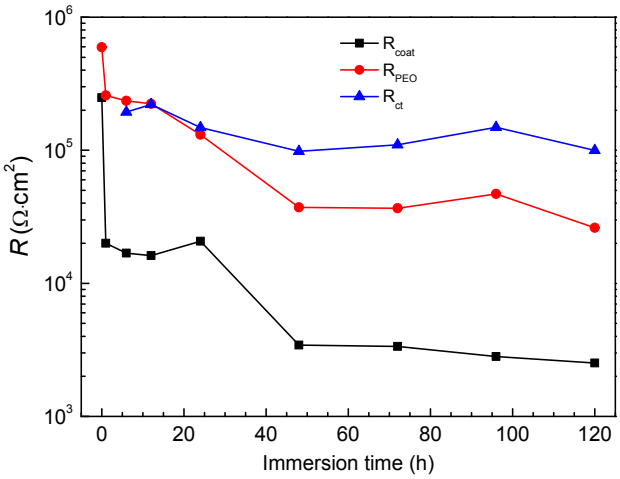

Fig. 6. The evolution of resistance values (obtained from EIS fitting results) with immersion in SBF at 37 ± 0.5 °C for the PEO-SHC.

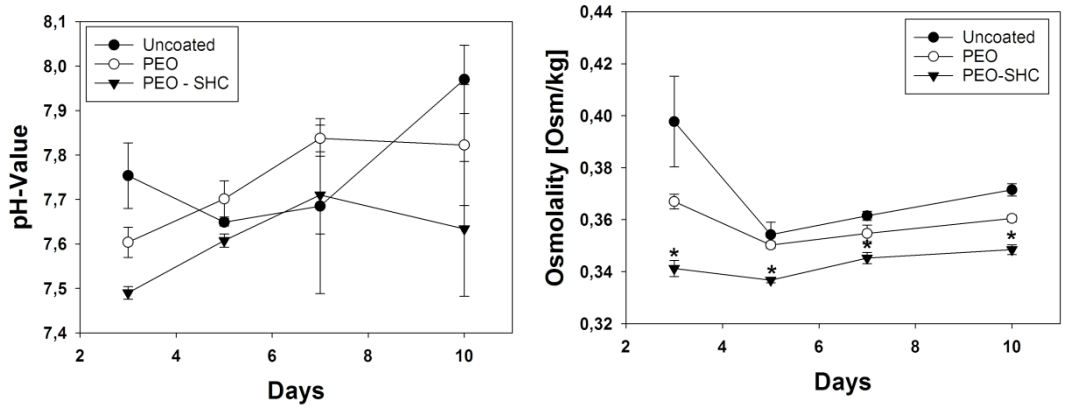

Fig. 7. pH (left) and osmolality measurements (right) performed at each medium change (Days 3, 5, 7 and 10). The asterisks indicate significant differences of the PEO-SHC to the uncoated specimen ($p<0.05$). Statistical analysis was done with ANOVA with Holm-Sidak post-hoc test.

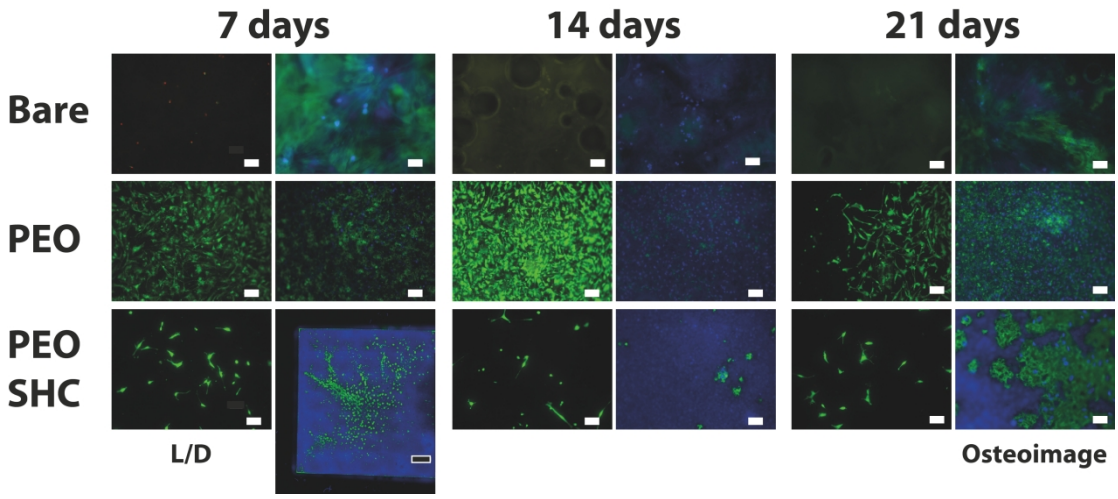

Fig. 8. Live/dead staining and determination of hydroxyapatite by Osteoimage (green) on the different samples, observed by fluorescence microscopy. White scale bars = 100 μm, black scale bar = 2000 μm.

Table 1 Chemical composition of the as received material.

Element	Ag	Al	Ca	Ce	Cu
wt.%	<0.00005	0.01400	<0.00010	<0.00040	0.00030

Element	Fe	La	Mn	Ni	Pb
wt.%	0.00620	<0.00050	0.01110	<0.00020	0.00164

Element	Si	Sn	Zn	Zr	Mg
wt.%	0.05910	0.00174	0.00690	<0.00050	99.90000

Table 2 Surface element composition of the bare magnesium, the PEO and PEO-SHC determined by EDS analysis.

Concentration (wt.%)	C	O	Na	Mg	Al	Si	P	K	Ca	Fe
Mg	-	1.91	-	98.09	-	-	-	-	-	-
PEO	5.63	46.08	2.69	23.48	2.19	6.34	12.41	0.21	0.36	0.62
PEO-SHC	65.07	26.06	-	-	-	-	-	-	8.87	-

Table 3 Electrochemical data of the samples as read from Fig. 3.

Samples	E_{corr} (V vs. SCE)	i_{corr} (A/cm^2)	E_{bd} (V vs. SCE)
Mg	-1.86 ± 0.01	(4.12 ± 0.40) × 10^{-5}	-
PEO	-1.92 ± 0.01	(9.22 ± 0.60) × 10^{-6}	-1.57 ± 0.01
PEO-SHC	-1.72 ± 0.01	(9.81 ± 0.50) × 10^{-9}	-1.32 ± 0.02

Highlights

(1) Super-hydrophobic coating decreases the substrate corrosion.

(2) PEO coating enhances human osteoblast proliferation, but not differentiation.

(3) Super-hydrophobic coating reduces osteoblast proliferation, but enhances differentiation.